

Determination of Differential Emission Measure from X-Ray Solar Spectra Registered by RESIK aboard CORONAS-F

A. Kepa^a, J. Sylwester^a, B. Sylwester^a, M. Siarkowski^a, and A. I. Stepanov^b

^aSpace Research Center, Polish Academy of Sciences, Kopernika 11, 51-622, Wrocław, Poland

^bPushkov Institute of Terrestrial Magnetism, Ionosphere, and Radio Wave Propagation, Russian Academy of Sciences, Troitsk, Moscow oblast, 142190 Russia

Received April 15, 2005

Abstract—The differential emission measure (DEM) describes the temperature distribution of the emitting plasma. The DEM distribution allows one to study the physical conditions and the energy of flares in detail (including the mean temperature and the total emission measure). In this paper, we analyze the time changes of the DEM distributions for a selected flare, which has been observed with the RESIK instrument. To calculate the differential emission measure, we used the Withbroe–Sylwester (W–S) iterative algorithm corresponding to the maximum likelihood procedure. The required emission functions were calculated with the CHIANTI package. We calculated the DEM for four available estimates of the ionization equilibrium and coronal composition of plasma.

PACS numbers: 96.60.Ub

DOI: 10.1134/S0038094606040058

INTRODUCTION

The differential emission measure $\varphi(T)$ characterizes the temperature distribution of the emitting plasma:

$$\varphi(T) = n_e^2 \frac{dV}{dT}, \quad (1)$$

where n_e is the plasma density, V is the plasma volume, and T is the temperature. The DEM distribution $\varphi(T)$ characterizes the amount of matter in the specified temperature interval (dT). Thus, the shape of the DEM distribution characterizes the physical conditions in the plasma. The distribution of the differential emission measure has already been studied for years based on measurements of fluxes in the X-ray and ultraviolet bands. To solve this inverse problem, various methods were used (Pottasch, 1964; Batstone et al., 1970; Dere et al., 1974). For the present calculations, we chose the Withbroe–Sylwester (W–S) iterative algorithm, a detailed description of which can be found in the paper by Sylwester et al. (1980). We have already used this method to study a flare observed with the RESIK instrument (Kepa et al., 2004). In the present study, we apply this method to analyze one of many observed flares. Here, we mostly concentrate on the influence of different ionization equilibrium approximations (used to calculate the theoretical fluxes in lines) on the resulting DEM distributions.

METHOD

The W–S algorithm is based on the maximum likelihood procedure. This is an iterative numerical method, in which the DEM φ_{j+1} distribution in iteration ($j+1$) is found from that in the preceding (j th) iteration using the correction factor c_i :

$$\varphi_{j+1}(T) = \varphi_j(T) \frac{\sum_{i=1}^k c_i w_i(T)}{\sum_{i=1}^k w_i(T)}. \quad (2)$$

The correction factor c_i depends on the ratio of the radiation flux observed in a given spectral line to that calculated from the previous DEM distribution (φ_j) and is determined by the formula

$$c_i = F_{oi}/F_{ci}, \quad (3)$$

where F_{oi} is the flux observed in the line i and F_{ci} is the flux calculated (for iteration j) by the formula

$$F_{ci} = \int_0^{\infty} f_i(T) \varphi_j(T) dT. \quad (4)$$

The theoretical dependences of the emission function f_i with the temperature in the line i are calculated using the CHIANTI package (Dere et al., 1997). The

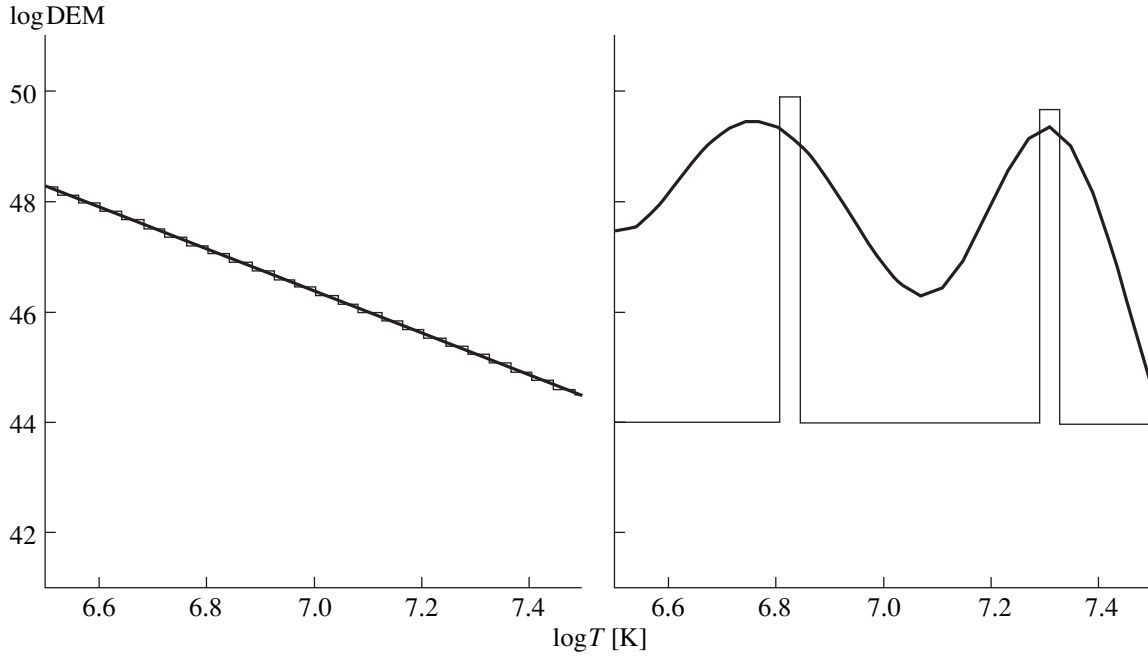


Fig. 1. The test of the method for building the DEM distribution: the results obtained with the W–S code. The synthetic and calculated models are shown with thin and thick lines, respectively. Left: the synthetic DEM model described with a power function. Right: the two-temperature synthetic model, for which the amounts of plasma at the temperatures 6.3 and 20 MK are the same.

emission functions describe the emissivity in a given line in plasma with a temperature T for a constant emission measure. In Eq. (2), the weight factor $w_i(T)$ is found from

$$w_i(T) = \frac{f_i(T)\phi_j(T) \int_0^\infty f_i(T)\phi_j(T)dT}{\int_0^\infty [f_i(T)\phi_j(T)]^2 dT} \times \left[\frac{|F_{oi} - F_{ci}|}{\delta_i} + 1 \right]^a, \quad (5)$$

where δ_i are the errors corresponding to the observations in the line i , and a is the optimization parameter.

The above method was checked, and tests confirmed its stability and capability to reconstruct the synthetic distributions specified in the temperature range from 5 to 30 MK (Fig. 1).

DATA

In the present study, we calculated the DEM distributions for flare of C8.1 X-ray class, which occurred close to the center of the solar disk (N14 E09) at 02:28 UT on January 21, 2003. Figure 2 displays the integrated spectrum of this flare (for about 1686 s) for four RESIK channels (3.3 Å–3.8 Å–4.3 Å–4.9 Å–6.0 Å). A detailed description of the RESIK spectrometer and its

calibration can be found in the paper by Sylwester et al. (2005). In Fig. 2, we have denoted the spectral regions whose radiation fluxes were used to calculate the DEM

Table 1. The spectral intervals and the corresponding main transitions

Number	Wavelength ranges (Å)	Main lines
1	3.340–3.368	Ar XVII $1s^2 \ ^1S_0 - 1s3p \ ^1P_1$
2	3.688–3.699	S XVI $1s \ ^2S_{1/2} - 5p \ ^2P_1$
3	3.724–3.740	Ar XVIII $1s \ ^2S_{1/2} - 2p \ ^2P_{1/2, 3/2}$
4	3.777–3.789	S XVI $1s \ ^2S_{1/2} - 4p \ ^2P_{1/2, 3/2}$
5	3.944–3.962	Ar XVII $1s^2 \ ^1S_0 - 1s2p \ ^1P_1 (w)$
6	3.963–3.980	Ar XVII $1s^2 \ ^1S_0 - 1s2p \ ^3P_{1,2} (x+y)$
7	3.981–4.004	Ar XVII $1s^2 \ ^1S_0 - 1s2s \ ^3S_1 (z)$
8	4.076–4.091	S XV $1s^2 \ ^1S_0 - 1s4p \ ^1P_1$
9	4.288–4.315	S XV $1s^2 \ ^1S_0 - 1s3p \ ^1P_1$
10	4.720–4.743	S XVI $1s \ ^2S_{1/2} - 2p \ ^2P_{1/2, 3/2} (Ly\alpha)$
11	5.030–5.061	S XV $1s^2 \ ^1S_0 - 1s2p \ ^1P_1 (w)$
12	5.086–5.124	S XV $1s^2 \ ^1S_0 - 1s2s \ ^3S_1 (z)$
13	5.204–5.232	Si XIV $1s \ ^2S_{1/2} - 3p \ ^2P_{1/2, 3/2} (Ly\beta)$
14	5.267–5.290	Si XIII $1s^2 \ ^1S_0 - 1s5p \ ^1P_1$
15	5.396–5.417	Si XIII $1s^2 \ ^1S_0 - 1s4p \ ^1P_1$
16	5.669–5.697	Si XIII $1s^2 \ ^1S_0 - 1s3p \ ^1P_1$

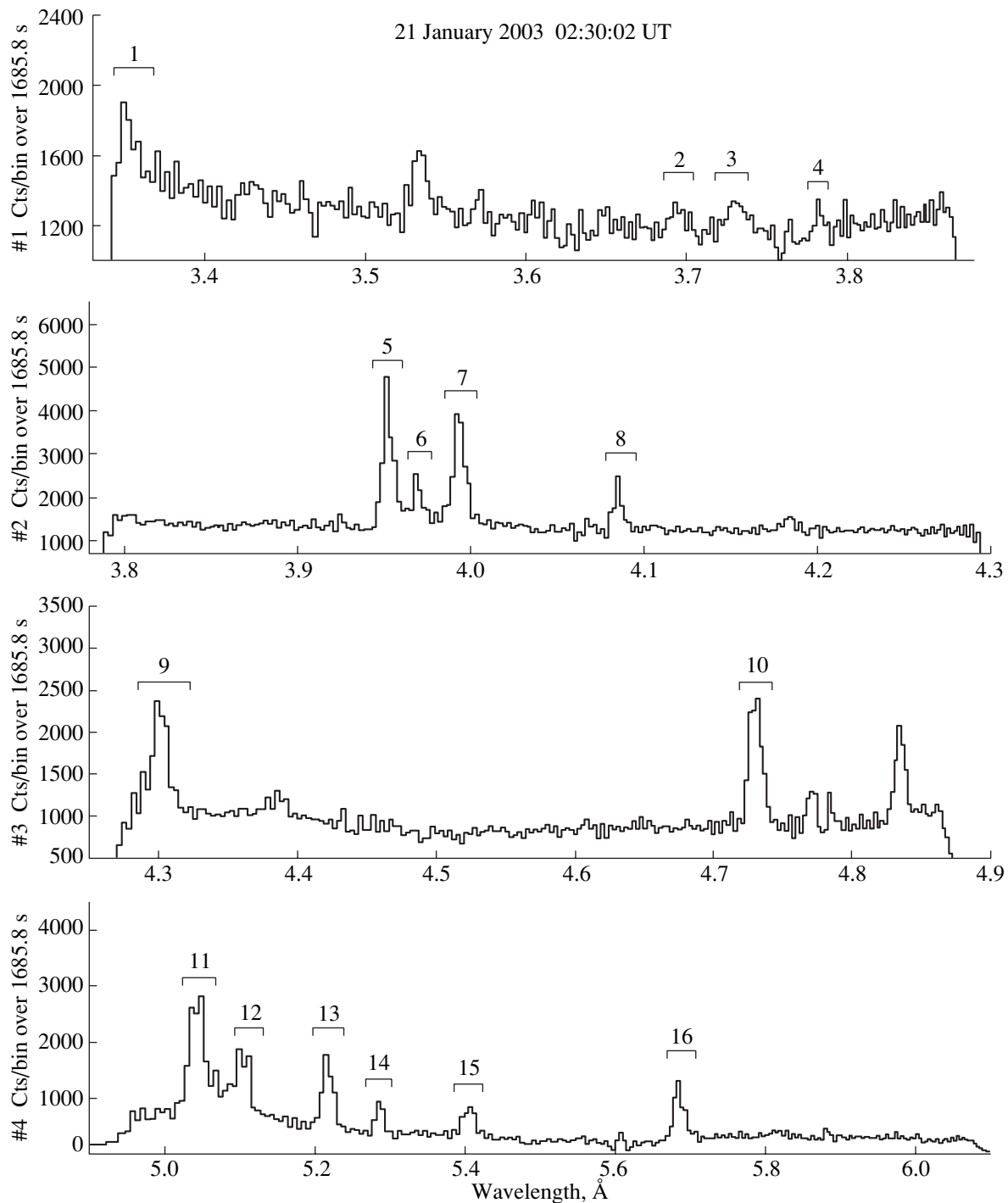


Fig. 2. The entire spectrum of the flare, which occurred on January 21, 2003, at 02:28 UT, obtained in four RESIK channels. The numbers (1–16) denote the spectral intervals which are given in Table 1 and are used to calculate the DEM distributions.

distributions. Table 1 presents the wavelength ranges covering the selected spectral lines and the corresponding main electron transitions contributing to the measured fluxes.

The lines of argon and sulfur are observed in the first and second channels. In addition, the potassium triplet

(3.53 Å) is observed in the first channel, but theoretical data on the corresponding emission functions are still lacking. In the third and fourth channels, the lines of sulfur and silicon are most pronounced. We specified 12 time intervals during the flare under consideration and calculated the fluxes in the spectral regions selected (using the data on the absolute calibration of the instru-

ment) with the corresponding errors for these intervals. These errors, necessary to calculate the DEM (the statistical error is assumed here to be equal to the square root of the number of registered photons), are rather small ($\leq 10\%$), because the sensitivity of the RESIK instrument is high. Using the measured fluxes (lines plus continuum in the selected spectral regions), we calculated the DEM distributions for the time intervals mentioned above. The intervals are given in Table 2 and in Fig. 3. The time behavior of the X-ray emission in the 1- to 8-Å range as observed by the *Geostationary Operational Environmental Satellite (GOES)* is also shown.

Figure 4 displays a three-dimensional diagram illustrating the time behavior of the fluxes in 16 selected spectral ranges (for 12 time intervals). Intervals 5 and 6 correspond to the phase of the flare maximum (Fig. 3). As is seen from Eq. (2), in order to calculate the DEM distribution, the theoretical temperature dependence of the line emissivity, the so-called emission function $f_i(T)$, is required. In our case, the required emission functions were calculated using the CHIANTI package (Dere et al., 1997) for 16 spectral ranges and for the coronal chemical composition of the Sun. Since we want to study the influence of the specified ionization equilibrium (IE) on the resulting DEM distribution, we calculated the emission functions $f_i(T)$ for four sets of the ionization equilibrium available in the literature: Shull–Steenberg (Shull and Steenberg, 1982), Arnaud–Rothenflug (Arnaud and Rothenflug, 1985), Arnaud–Raymond (Arnaud and Raymond, 1992), and Mazzotta (Mazzotta et al., 1998). The temperature behavior of the emission functions obtained with the four sets of IE is shown by different symbols in Fig. 5. It is seen that $f_i(T)$ are generally the same with only small differences. The results obtained with the IE estimates from Shull–Steenberg and Mazzotta differ most.

RESULTS OF DEM CALCULATIONS

The DEM distributions for the selected flare calculated with the technique described above are displayed in Fig. 6. These results were obtained with a set of four ionization equilibrium (IE) estimates and are shown for different phases of the flare evolution (intervals 1 and 2, corresponding to the rise phase, are shown in the top panels; intervals 5 and 6, corresponding to the maximum phase, are presented in the middle panels; and intervals 11 and 12, corresponding to the decay phase, are demonstrated in the bottom panels). As might be expected, the DEM distributions obtained with the ionization equilibrium estimates from Shull and Steenberg differ from the others most. However, the general shape of the DEM distribution is the same regardless of the method applied for IE calculations. In most cases, the DEM distribution can be considered as two-compo-

Table 2. The time intervals for which the spectral fluxes of the X-ray radiation of the analyzed flare (January 21, 2003) were obtained

Number	Intervals
1	02:25:04 UT – 02:26:06 UT
2	02:26:06 UT – 02:26:40 UT
3	02:26:40 UT – 02:27:06 UT
4	02:27:06 UT – 02:27:36 UT
5	02:27:36 UT – 02:28:10 UT
6	02:28:10 UT – 02:28:44 UT
7	02:28:44 UT – 02:29:24 UT
8	02:29:24 UT – 02:29:58 UT
9	02:29:58 UT – 02:30:40 UT
10	02:30:40 UT – 02:32:02 UT
11	02:32:02 UT – 02:34:12 UT
12	02:34:12 UT – 02:38:36 UT

nent. One component corresponds to the cold plasma with temperatures ranging from 5 to 10 MK. The second component corresponds to the hotter plasma with a maximum temperature of about 20 MK. The position of this maximum and its height depend on the flare phase.

Since the calculated DEM distribution only slightly depends on the choice of the IE approximation, for fur-

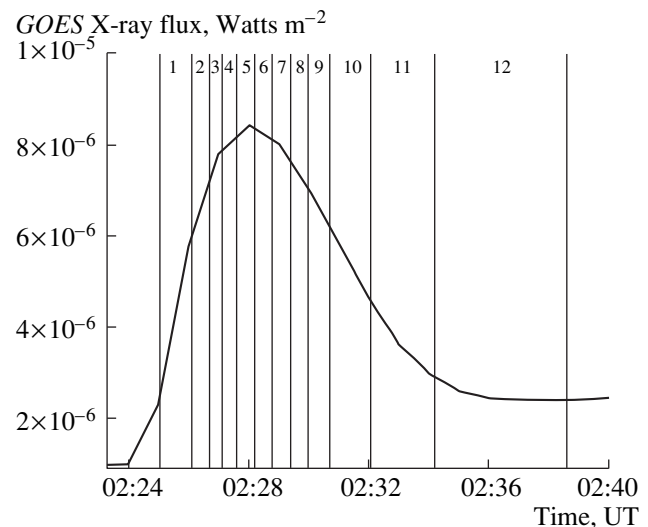


Fig. 3. The time behavior of the X-ray flux (1–8 Å) observed with *GOES* during the flare under consideration. The numbers at the top denote the intervals for which the DEM distributions were calculated.

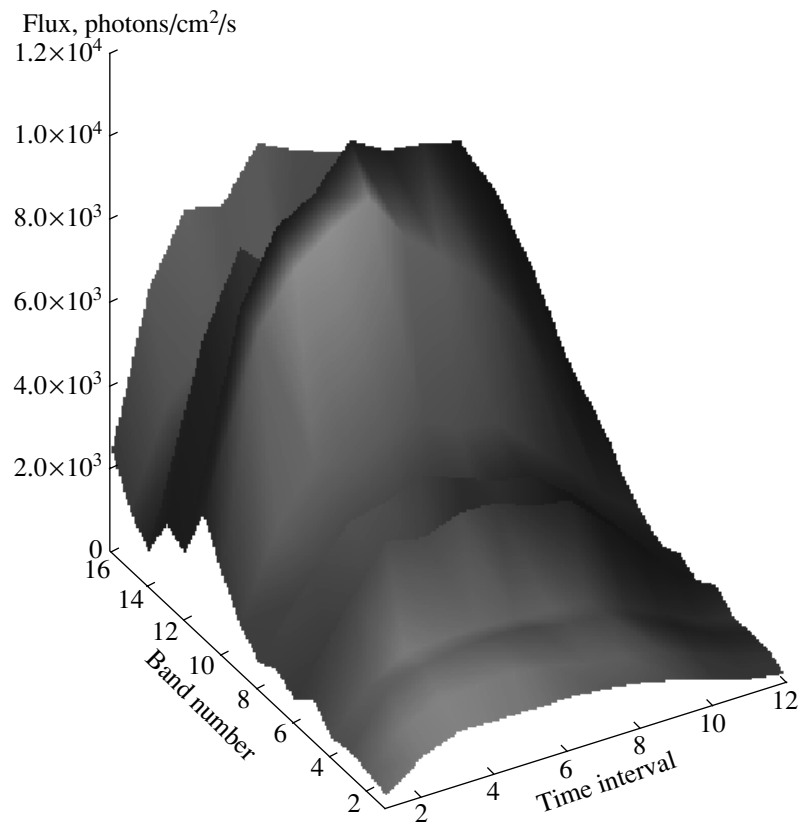


Fig. 4. A three-dimensional diagram displaying the time behavior of the absolute fluxes in the observed selected intervals.

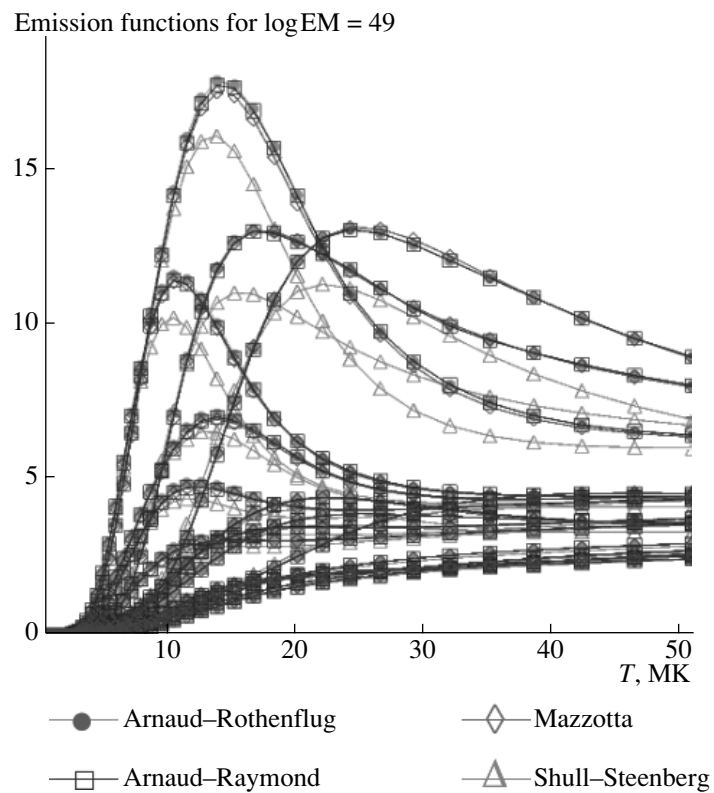


Fig. 5. The emission functions $f_i(T)$ of the selected lines calculated for four different estimates of the ionization equilibrium.

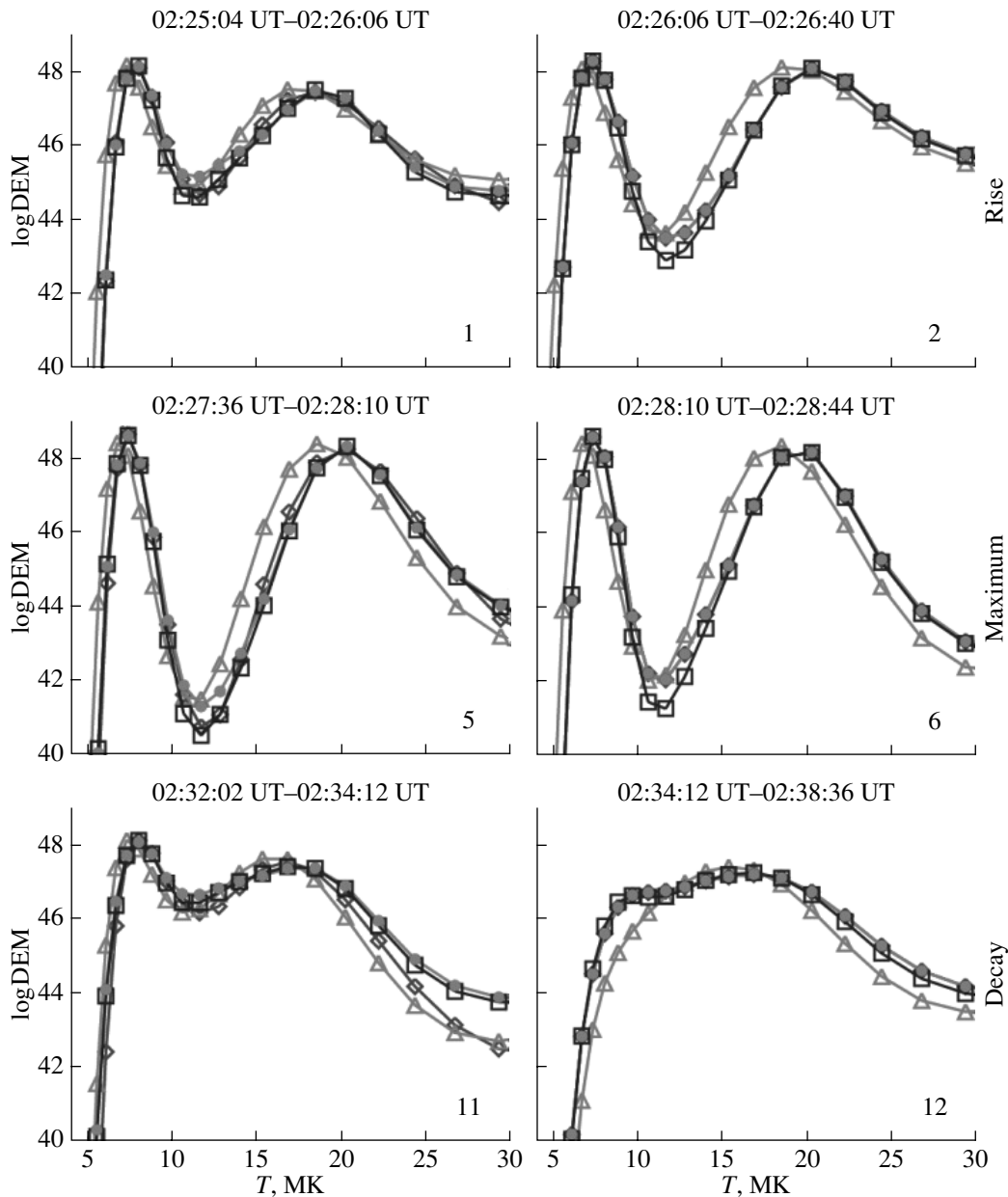


Fig. 6. Examples of the DEM distributions calculated for different moments of the Jan. 21, 2003, flare evolution.

ther analysis, we choose the calculations based on the IE estimate from Mazzotta. This estimate is also used most extensively in the literature.

To get an idea of the “quantitative” dependence of the individual components of the DEM distribution with time, we selected three components of plasma at temperatures from 5 to 30 MK: (A) the cold plasma component (with temperatures $T < 10$ MK), (B) the component with moderate temperatures ($10 \text{ MK} < T < 20$ MK), and (C) the hot component (with temperatures above 20 MK). Figure 7 shows the time behavior of the emission measure of the considered flare in the temper-

ature subranges mentioned above. The temporal variations are quite similar for components A and B, i.e., for the plasma with temperatures below 20 MK. The amount of this plasma weakly changes with time during practically the whole flare (~ 10 min). For the hot component C, the emission measure constantly decreases from the very beginning of the event: all the points except the first one lie along a single straight line.

For the twelve selected intervals covering all phases of this event, the evolution of the DEM distribution obtained with this IE estimate is shown in Fig. 8.

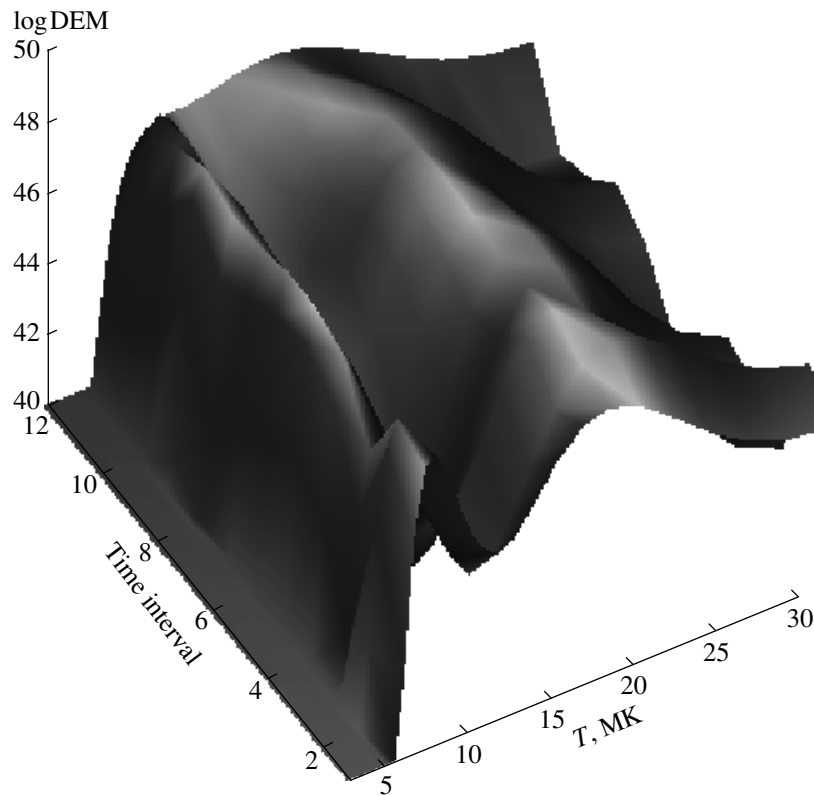


Fig. 7. The evolution of the DEM distributions for the ionization equilibrium given in the paper by Mazzotta et al. (1998).

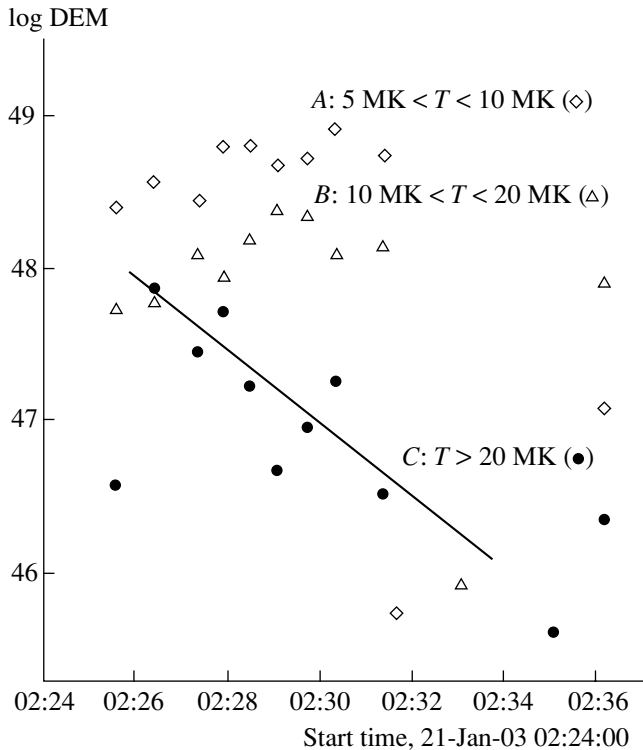


Fig. 8. The time variations of the emission measure of the hot and cold plasma components during the flare of January 21, 2003.

CONCLUSIONS

The analysis of calculations of the differential emission measure (DEM) distributions made for the selected flare (January 21, 2003) allows us to conclude the following:

(1) The temperature behavior of the DEM distribution weakly depends on the approximations used for the ionization equilibrium.

(2) The DEM distributions obtained based on the measurements of solar radiation fluxes in the spectral lines observed with the RESIK instrument are two-component. The cold (low-temperature) and hot (high-temperature) components of the distribution correspond to plasma with temperatures ranging from 5 to 10 MK and from 15 to 25 MK, respectively.

(3) During a flare's evolution, the emission measure in the hot and cold components behaves quite differently. The amount of the hot plasma decreases quickly, while the amount of the cold plasma is almost constant (it decreases only at the end of the decay phase).

ACKNOWLEDGMENTS

The authors are grateful to all participants of the *CORONAS-F* project and to colleagues from the Pushkov Institute of Terrestrial Magnetism, the Ionosphere, and Radio Wave Propagation, Russian Academy of Sci-

ences, whose assistance made possible the success of the Polish experiments on the *CORONAS-F* satellite.

This study was supported by the Polish Ministry of Education and Science (grant no. 1.P03D.017.29).

REFERENCES

- Arnaud, M. and Rothenflug, R., An Updated Evaluation of Recombination and Ionization Rates, *Astron. Astrophys.*, 1985, vol. 60, pp. 425–457.
- Arnaud, M. and Raymond, J.C., Iron Ionization and Recombination Rates and Ionization Equilibrium, *Astrophys. J.*, 1992, vol. 398, pp. 394–406.
- Batstone, R.M., Evans, K., Parkinson, J.H., and Pounds, K.A., Further X-Ray Spectra of Solar Active Regions, *Sol. Phys.*, 1970, vol. 13, pp. 389–400.
- Dere, K.P., Horan, D.M., and Kreplin, R.W., A Multi-Thermal Analysis of Solar X-Ray Emission, *Sol. Phys.*, 1974, vol. 36, pp. 459–472.
- Dere, K.P., Landi, E., Mason, H.E., et al., CHIANTI—An Atomic Database for Emission Lines, *Astron. Astrophys.*, 1997, vol. 125, pp. 149–173.
- Kepa, A., Sylwester, J., Sylwester, B., and Siarkowski, M., First Determinations of Differential Emission Measure Distribution from RESIK X-Ray Spectra, *Proc. IAU Symp. No. 233*, 2004, pp. 461–462.
- Mazzotta, P., Mazzitelli, G., Colafrancesco, S., and Vittorio, N., Ionization Balance for Optically Thin Plasmas: Rate Coefficients for All Atoms and Ions of the Elements H to NI, *Astron. Astrophys.*, 1998, vol. 133, pp. 403–409.
- Pottasch, S.R., On the Interpretation of the Solar Ultraviolet Emission Line Spectrum, *Space Sci. Rev.*, 1964, vol. 3, pp. 816–855.
- Shull, J.M. and van Steenberg, M., The Ionization Equilibrium of Astrophysically Abundant Elements, *Astrophys. J., Suppl.*, 1982, vol. 48, pp. 95–107.
- Sylwester, J., Schrijver, J., and Mewe, R., Multitemperature Analysis of Solar X-Ray Line, Emission, *Sol. Phys.*, 1980, vol. 67, pp. 285–309.
- Sylwester, J., Gaicki, I., Kordylewski, Z., et al., RESIK: A Bent Crystal X-Ray Spectrometer for Studies of Solar Coronal Plasma Composition, *Sol. Phys.*, 2005, vol. 226, pp. 45–72.